High-Q and temperature stable photonic biosensor based on grating waveguides

Sourabh Sahu[1*], Jalil Ali[2], Preecha P. Yupapin[3,4], Ghanshyam Singh[1] and K. T. V. Grattan[5]
[1]Department of Electronics and Communication Engineering, Malaviya National Institute of Technology, Rajasthan, (INDIA)
[2]Laser Centre, IBNU SINA ISIR, Faculty of Science, Universiti Teknologi Malaysia, 81310 Johor Bahru, (MALAYSIA)
[3]Computational Optics Research Group, Advanced Institute of Materials Science, Ton Duc Thang University, District 7, Ho Chi Minh City, (VIETNAM)
[4]Faculty of Electrical & Electronics Engineering, Ton Duc Thang University, District 7, Ho Chi Minh City, (VIETNAM)
5 City Graduate School and School of Mathematics, Computer Science & Engineering, City, University of London, London, EC1V 0HB, (UNITED KINGDOM)
sourabh.ggits@gmail.com, gsingh.ece@mnit.ac.in

Abstract. In this work, analytical modeling and parameter evaluation of a photonic biosensor using cascaded silicon grating waveguides is illustrated. The sensor design consists of two cascaded waveguides with symmetric sidewall gratings to broaden the stop band region of the transmission spectra. In the work, the structure is first analyzed using the transfer matrix method. The parameter values are then optimized to obtain a sharper resonant peak in the center of the stop band. Notably, the resonant band of this structure provides a high Q factor (of 1.544×10^5), which significantly improves the limits of detection. The sensor has been designed to detect the presence of biomaterial material (seen corresponding to a change in refractive index) on its surface by changing the change in device resonant wavelength. In this study, the effect of temperature on the detection of such biomaterials has also been evaluated, as has the temperature sensitivity of the device which is -0.0075nm/^{o}C, over a temperature range of 18 ^{o}C to 34 ^{o}C.

Keywords: biosensor, transfer matrix method, Sellemeier equation, biochemical sensor.

1 Introduction

The advent of silicon photonics has seen an exponential growth in the development of photonic devices for applications focussed on biomedical diagnostics, environmental and safety monitoring, military surveillance and many more such areas of interest. For medical diagnostics, photonic devices are used extensively for biochemical detection in smart healthcare as indicators, for example (Fan et al. 2008; Zinoviev et al. 2008). The advantages of photonic biosensors are high sensitivity, compact size, robustness, freedom from electromagnetic interference and ease of fabrication using existing CMOS fabrication facilities. Photonic biosensors can conveniently be classified as two main types: labeled and label-free. In the labeled sensor, radioactive or fluorescent particles for example are attached to the targeted material as indicators, and a laborious and complex quantitative analysis is performed for a precise prediction of the biomaterial performance. Such a technique is, in general, highly sensitive but the attachments of fluorescent particles can cause them to react with other biomolecules present that may then cause fluctuations in the overall output and therefore an error in the sensor response when compared to the original calibration. The most advanced method of detection is based on the label-free approach as such

problems are avoided and in the label-free method, a specific biorecognition coating is needed at the surface of a sensor, that can only attach or bind to the dedicated molecule. The binding phenomenon changes the physical properties that then modify the optical characteristics of the photonic device (Fan et al. 2008; Zinoviev et al. 2008; Estevez et al. 2012). Based on these factors, a number of researchers have investigated the capability of the photonic sensors. The most frequently reported work has been concentrated on surface plasmons resonance (Chiu et al. 2005; Ni et al. 2015; Azzam et al. 2016; Mohanty et al. 2015), disk resonators (Boud et al. 2001; Guider et al. 2015), photonic crystal based devices (Dutta and Pal 2013; Derbali et al. 2011), and interferometers (Liu et al. 2013; Sahu et al. 2016). Further, the response of a Surface Plasmon resonance (SPR) sensor device is strongly dependent on the quality of the deposited material, especially the thickness and roughness of the coating. Additional modifications are also required in sensors of this type where an enzyme coating is used for the quantization of the complex biomaterials. However, the interference often seen due to the presence of a large number of whispering gallery modes limits the usability of ring and disk resonators for biosensing applications, apart from which the ring resonator devices also suffers from bending losses. The interferometric biosensors appear on the whole to be highly sensitive, but the direct dependency of the sensitivity on the unbalanced arm length increases the overall dimensions of the device, and even then a low Q-factor and sinusoidal variation at the output limits its usability as an effective sensing device. The class of photonic crystal-based devices provide higher Q factor and improved limits-of-detection, but such sensors require a complex manufacturing process to allow the precisely fabricated dimensions needed for such devices and they also show higher propagation losses. When compared to other photonic biosensors, the Bragg Grating-based resonating device suffers from transmission losses which are linked to the device construction. The size of the smallest feature of the structure (for example the depth of a grating) is more prone to fabrication variability (Chen et al. 2015; Sahu et al. 2017; Wang et al. 2013; Sahu and Singh 2017; Prabhathan et al. 2009). Despite that, such a design provides several advantages such as high Q factor, single-mode cavity, robust and the ability of integration for lab-on-chip (LOC) applications.

Grating-based resonator structures have the capability of providing high sensitivity and a low limit of detection (Wang et al. 2013). The structure typically utilizes the conventional slab waveguide approach in which the mode is concentrated on the high index core region that is extended to sidewalls of the waveguide. The small deformity on the sidewall is replicated by changing the optical characteristics of the structure. In that way, the Bragg structure can be designed by periodically adjusting the waveguide width that correspondingly changes the effective refractive index. This periodic change in the effective index is the basis of the stop band region on the transmission spectra and such a structure can further be exploited for the creation of a sharp resonating band by placing a cavity at the center of the periodic grating structure (Prabhathan et al. 2009; Chrostowski and Hochberg 2015; Prabhathan and Murukeshan 2014). The shift of the band corresponding to a change in the surface biomaterial can be utilized for biosensing applications. It operates as follows: a binding event of the molecules perturbs the surface refractive

index of the sensor, resulting in a shift in the resonant wavelength. Such photonic sensors are highly sensitive, and can easily detect and differentiate the minimal changes in refractive index required to be monitored by promoting a greater interaction between the light and the biomaterial. Prabhathan et al. (Prabhathan and Murukeshan 2014) have demonstrated high Q and highly sensitive Bragg grating biosensors based on a phase-shift cavity resonator. Samira et al. (Najafgholinezhad and Olyaee 2014) have shown the temperature stability of such photonic sensors by considering the temperature varying microfluidic framework.

In this paper, the extraordinary ability of grating waveguide structures for a specific biosensing application is discussed. The structure discussed is composed of two cascaded grating waveguides, which widen the stop band region in the transmission spectra and the optimized cavity between the two waveguides produces a sharp resonant peak, of the order of $Q \sim 10^5$. Further, the important effect of the variation of the temperature on the upper cladding surface is also studied. The paper is structured as follows: Sec. 2 presents the theory and analytical modeling of Bragg grating structure, Sec. 3 depicts device structure and discusses the methodology to model stopband. Ther evaluation of bio-sensing parameters is described in Sec. 4. The temperature dependence of the defect cavity has been investigated and is discussed in Sec. 5. Finally, Sec. 6 discusses the conclusions drawn from this study and extensive reference to the literature is made.

2 Analytical modeling of a grating waveguide

A schematic of a single grating segment is shown in Fig. 1. The optical signals used, when propagated through the structure, suffer reflections at all the interfaces. After many simultaneous reflections, only those signals that go through constructive interference are enhanced, while others cancel and propagate through gratings of a waveguide such as this. The reflected signals are observed in the transmission spectra in the form of stopband (Chrostowski and Hochberg 2015).

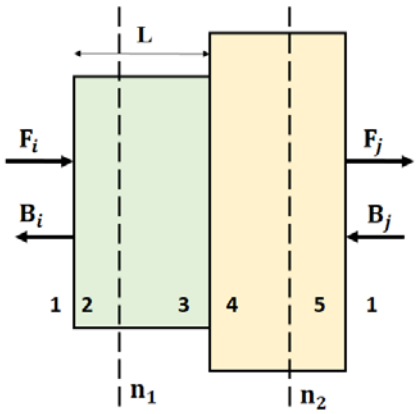

Fig. 1 Layered structure (single grating segment of a waveguide) used for TMM calculation

The output response of cascaded grating waveguides (CGW) is analytically evaluated through the transfer matrix method (TMM). The TMM is a prefered method for analyzing high index contrast

periodic structures such as this. Here the signal propagation in the interface 1-2 (step index) is represented by the reflection and transmission coefficient, which is evaluated through consideration of Fresnel's equation of reflection $(n_2 - n_1)/(n_2 + n_1)$ (Chrostowski and Hochberg 2015), where n_1 and n_2 are the effective refractive indices of the waveguide segments, as shown in Fig. 1. The corresponding matrix representation is given by;

$$\begin{bmatrix} F_2 \\ B_2 \end{bmatrix} = \begin{bmatrix} 1/t & r/t \\ r/t & 1/t \end{bmatrix} \cdot \begin{bmatrix} F_1 \\ B_1 \end{bmatrix} = \begin{bmatrix} \frac{n_1+n_2}{2\sqrt{n_1 \cdot n_2}} & \frac{n_1-n_2}{2\sqrt{n_1 \cdot n_2}} \\ \frac{n_1-n_2}{2\sqrt{n_1 \cdot n_2}} & \frac{n_1+n_2}{2\sqrt{n_1 \cdot n_2}} \end{bmatrix} \cdot \begin{bmatrix} F_1 \\ B_1 \end{bmatrix} = M_{1-2} \cdot \begin{bmatrix} F_1 \\ B_1 \end{bmatrix} \quad (1)$$

Similarly, the matrix representation of the signal propagating from segment 2-3 (homogeneous waveguide) can be given as:

$$\begin{bmatrix} F_3 \\ B_3 \end{bmatrix} = \begin{bmatrix} e^{-j\beta L} & 0 \\ 0 & e^{j\beta L} \end{bmatrix} \cdot \begin{bmatrix} F_2 \\ B_2 \end{bmatrix} = M_{2-3} \cdot \begin{bmatrix} F_2 \\ B_2 \end{bmatrix} \quad (2)$$

where β is a propagation constant considering effective index and propagation loss (α) and L is the length of the layer.

The overall matrix representation of the complete structure (M_{BG}), shown in Fig. 1 can then be given as:

$$M_{BG} = M_{1-2} M_{2-3} M_{3-4} M_{4-5} \quad (3)$$

Thus the matrix representation of the complete grating waveguide with N number of grating periods can be represented by:

$$M = (M_{BG})^N \quad (4)$$

3 Cascaded grating waveguide (CGW) and stopband modeling

The proposed structure of a CGW design is shown in Fig. 2. The structure is drawn on a silicon-on-insulator (SOI) platform, the thickness of the core region is 220 nm and it is placed between the 2 μm thick silicon substrate and the upper cladding region. The material used for the core and the cladding regions are Si and SiO_2 having a refractive indices values of 3.47 and 1.444 respectively, at 1550 nm. The evaluation of the fundamental modes is undertaken using a finite difference based Eigen-mode solver approach. Although several modes are found, according to a requirement to produce a wide stopband here, the fundamental quasi-TE mode is considered. The field concentration of the TM mode is mostly on the surface of the waveguide, that causes a very low interaction with the corrugated sidewall of the waveguide. So this produces a very narrow stop band region that too was found for the significantly large number of grating periods (Chen et al. 2015) seen. In the design of the grating waveguide, the phase matching condition needs to be verified, which corresponds to an evaluation of the grating period (Λ). The relationship is given by $\Lambda = \frac{\lambda_B}{2 \cdot n_{eff}}$, where λ_B is the Bragg wavelength, and n_{eff} is the average value of the effective refractive index of the waveguide layers (Fig. 1). The value of the Λ depends on the value of the effective refractive index. Thus, Λ is lower for the TE mode than for the TM mode waveguide: hence the overall length of the grating waveguide is also less for the TE mode operated grating

waveguide (Wang et al. 2013; Sahu and Singh 2017; Prabhathan et al. 2009). The grating period has a strong influence on the coupling of the signals. If a grating period, $\Lambda > \lambda_B/(2\cdot neff)$, then the region is suitable for designing a fiber to waveguide coupler. In this region light, after interacting with the structure width, experiences scatter caused by discontinuity and becomes weak and is radiated out (Gonzalo Wangüemert-Pérez et al. 2014). Generally, fiber to waveguide grating couplers have been designed to work under this operating condition. Secondly, the region where $\Lambda < \lambda_B/(2\cdot neff)$, is called as a sub-wavelength region, in which the waveguide is ideally lossless (Gonzalo Wangüemert-Pérez et al. 2014a; Wang et al. 2014).

A method discussed in Sec.2 is used to evaluate the transmission spectra of the structure (Fig. 2). The value of the propagation loss considered is 3 dB/cm (Chen et al. 2015; Wang et al. 2013; Chrostowski and Hochberg 2015). The device consists of three segments, where the first and the second segment of the device consist of grating waveguides with their corrugation widths given by ΔW_1 and ΔW_2 (Fig. 2a). The number of the grating idividual segments is set to N = 375. Based on the results shown in Fig. 3, it is found that the individual grating waveguides provide a stop band in the range of 1.53459 – 1.54452μm for ΔW_1 (Fig. 3a) and 1.54288 – 1.55021μm for ΔW_2 (Fig. 3b). The transmission spectra of the overall device show a band gap region of 1.53459 – 1.55021μm which is greater than the band gap found for the individual grating waveguides (Fig. 3c).

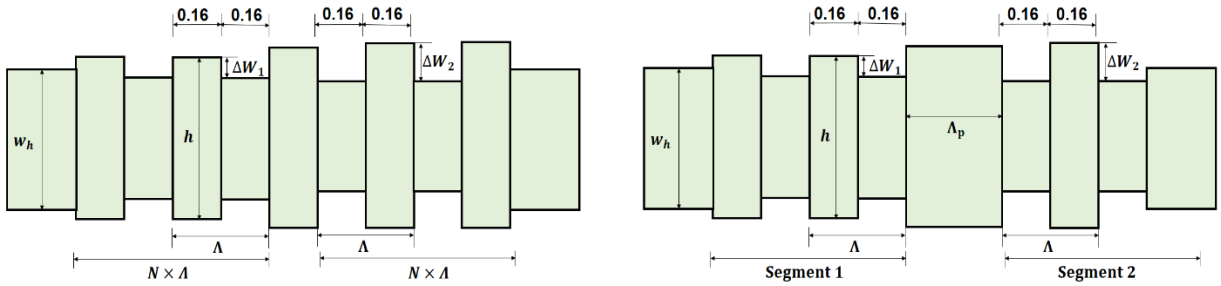

(a) (b)

Fig. 2 Cascaded grating waveguide with **a** corrugation of ΔW_1 and ΔW_2, and **b** with a cavity defect.

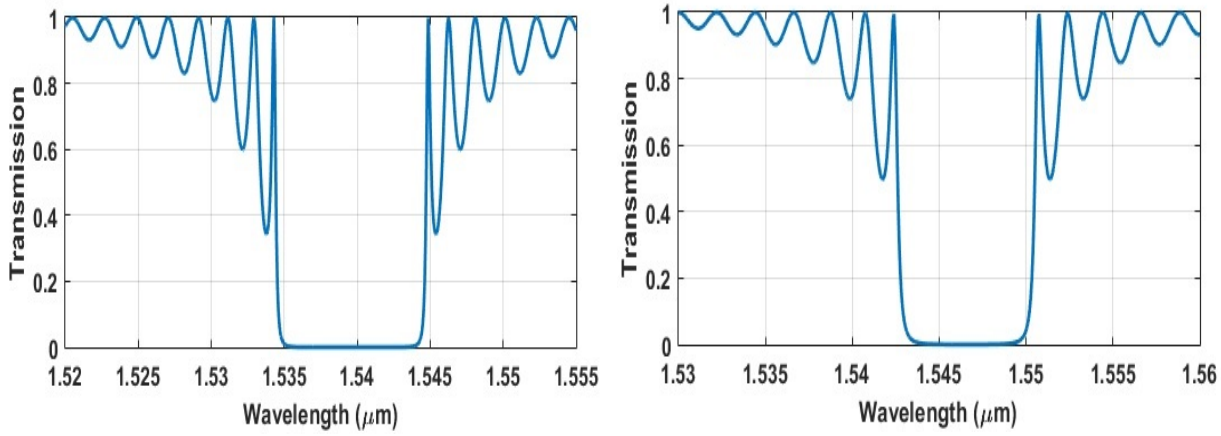

(a) (b)

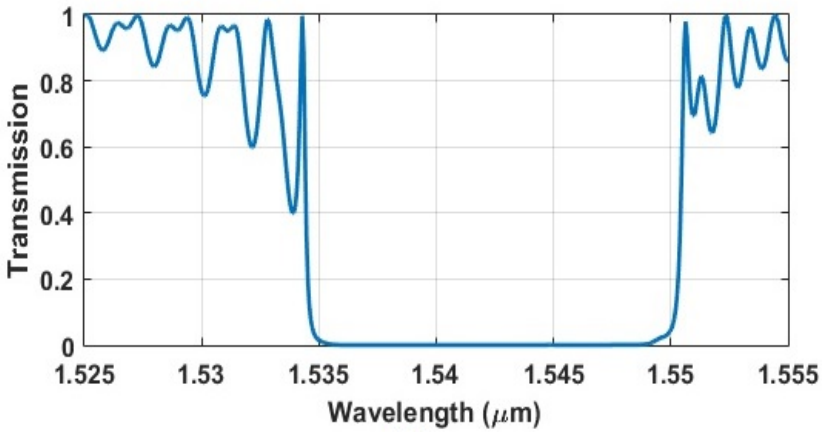

(c)

Fig. 3 Individual transmission spectra of the grating waveguide **a** Segment 1, **b** Segment 2 and **c** cascaded waveguide

Table 1 Geometric parameters of the structure shown (Fig. 2)

Parameters	**Value**
$\mathbf{w_h}$	0.50 μm
h	0.52 μm
Λ	0.32 μm
$\mathbf{\Delta W_1}$	0.04 μm
$\mathbf{\Delta W_2}$	0.06 μm
$\mathbf{\Lambda_p}$	0.34 μm
N	375

The various geometric parameters of the structure considered are listed in Table 1. The corresponding matrix representation is given by $M = (M_{BG1})^N \cdot (M_{BG2})^N$. Out of the three segments, the third segment represents a defect cavity of length Λ_p, shown in Fig. 2b. On account of the insertion of the cavity between the two grating waveguides, a sharp resonant peak occurs in the center of the stop band region, as is seen i Fig. 4a. The modified matrix representation is given by $M = (M_{BG1})^N \cdot M_{cavity} \cdot (M_{BG2})^N$, where the homogeneous waveguide segment is considered in the calculation of M_{cavity}. Transmission spectra of the full device are shown in Fig. 4a-b which shows the close up of the resonant wavelength. The spectacular sharp resonant peak for $\Delta\lambda_{FWHM}$ (full width at half maxima) of 0.01 nm is observed at 1.544 microns. The measured quality factor (Q-factor) on this basis is 1.544×10^5, which is very high and is important to be utilized for applications such as multiplexing and sensing.

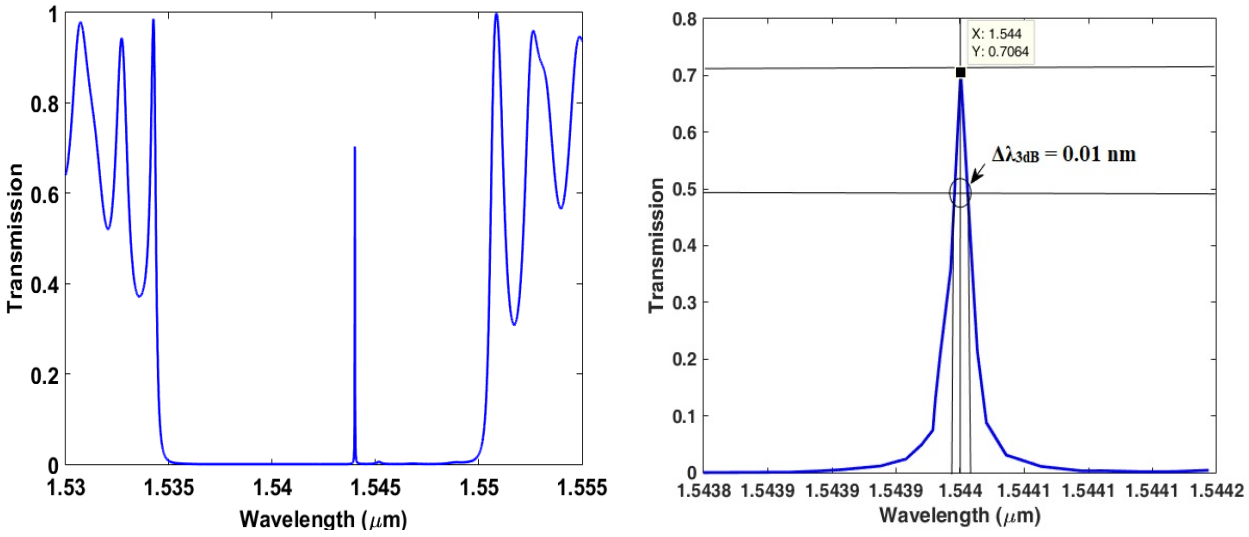

(a) (b)

Fig. 4 a Transmission spectra of the complete structure with a defect at the center of a waveguide, **b** zoomed version of the resonant peak.

4 Characteristics which are important for biosensing applications

Based on the above discussion, the capacity of the device for the biosensing applications is evaluated and opportunities discussed. The microfluidic framework responsible for supplying biomaterials to the surface of the sensor is considered in the top part of the structure, which is the upper cladding region. For a device to be highly sensitive requires a larger variation in the effective index of a waveguide for a given change in refractive index of a biomaterial. In this work the considered biomaterials (and their refractive index (RI) values) are distilled water (RI = 1.33), Hemoglobin (RI = 1.38), Biotin-Streptavidin (RI = 1.45), and Bovine Serum Albumin (RI = 1.47).

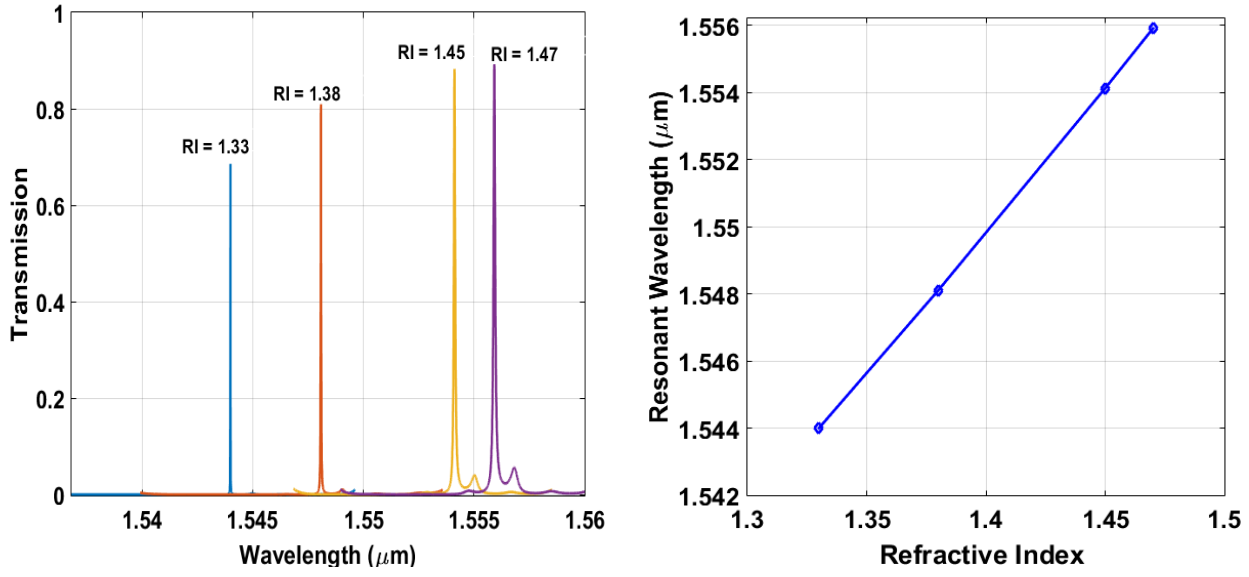

(a) (b)

Fig. 5 a Transmission spectra, **b** resonant wavelength shift as a function of the change in refractive index.

By changing the biomaterial, a significant shift in the resonant wavelength (λres) can be observed in the spectra obtained from the device, as shown in Fig. 5a. Fig. 5b represents the linear relationship between the resonant wavelength (λ_{res}) and n_c. From the graph, it can be observed that the resonant wavelength has shifted from 1554.02 at n_c = 1.33 to 1556.13 at n_c = 1.47. The key performance parameters of the photonic biosensors to be optimized are sensitivity and limit of detection. The sensitivity is defined as, $S = (\Delta\lambda_{res}/\Delta n_c)$ where $\Delta\lambda$ represents a shift of resonant wavelength and it is evaluated from the slope of Fig. 5b. The limit of detection (Δn_{min}) is the minimum possible resolution of n_c required to obtain an observable shift in the resonant wavelength. The evaluation of various key device parameters is performed by adopting the procedures defined in the literature (Talebi et al. 2013; Wang et al. 2013). Theoretical determination of the device sensitivity is 90 nm/RIU (where RIU is refractive index unit). The normalized sensitivity was determined to be 0.0583 /RIU with a LOD of 1.1184×10^{-4} RIU.

5 Temperature dependence of the structure

The materials used have a significant impact on device performance due to the variation of environmental temperature, which also alters the response of the device. To improve the consistency in this response, several practical factors should be considered. Most biological fluids have a significant proportion of water – indeed it is the main component present in blood plasma, extracellular fluid, etc., so studying the effect of changes in temperature of water on the response of the designed photonic sensor is important for many biosensing applications. Based on the previously reported literature it has been found that the wavelength shift and the temperature dependent refractive index of water can be found using Eq. (5) (Bashkatov and Genina 2003) where:

$$n(\lambda, t) = A(t) + \frac{B(t)}{\lambda^2} + \frac{C(t)}{\lambda^4} + \frac{D(t)}{\lambda^6} \quad (5)$$

and λ= 1550 nm is the wavelength of light.

$$A(t) = 1.3208 - 1.2325 \times 10^{-5}t + 1.8674 \times 10^{-6}t^2 + 5.0233 \times 10^{-9}t^3 \quad (6)$$

$$B(t) = 5208.2413 - 0.5179t - 2.284 \times 10^{-2}t^2 + 6.9608 \times 10^{-5}t^3 \quad (7)$$

$$C(t) = -2.5551 \times 10^{8} - 18341.336t - 917.2319t^2 + 2.7729t^3 \quad (8)$$

$$D(t) = 9.3495 + 1.7855 \times 10^{-3}t + 3.6733 \times 10^{-5}t^2 - 1.2932 \times 10^{-7}t^3 \quad (9)$$

where t (°C) is the temperature.

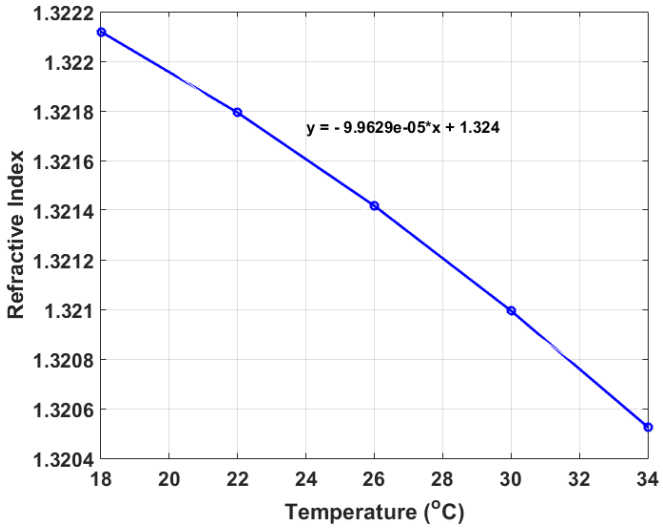

Fig. 6 Change in refractive index due to changes in temperature.

In this work, the narrow temperature range 18 ºC to 34 ºC in which water molecules exist in the biomaterials has been considered. From Fig. 6, it is observable that the water has a negative temperature coefficient, that decreases its refractive index and hence this is seen to vary the resonant wavelength of the device.

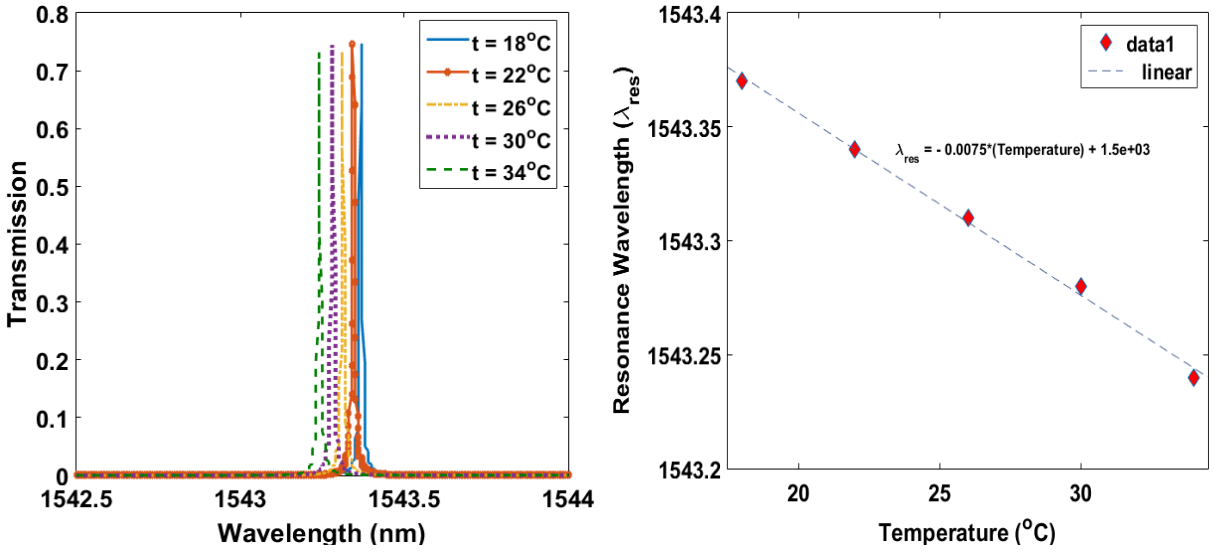

(a) (b)

Fig. 7 (a) Transmission spectra of structure for change in temperature, (b) shift in resonant wavelength (in terms of nm) due to change in temperature.

Table 2 Value of refractive index and resonant wavelength for variation of temperature.

Temperature (ºC)	Refractive Index	Resonant Wavelength (nm)
18	1.3221	1543.37
22	1.3218	1543.34

26	1.3214	1543.31
30	1.3210	1543.28
34	1.3205	1543.24

In Fig. 7a the shift in a resonant wavelength corresponding to temperature variation is shown. An almost linear behaviour of the relationship has plotted in Fig. 7b and the evaluated temperature sensitivity is found to be -0.0075 nm/^{o}C – a figure that indicates only 0.12 nm wavelength shift over the specified temperature range. Table 2 presents the refractive index and resonant wavelengths that correspond to a change in temperature. The proposed structure is simple to design and can be fabricated by a conventional CMOS fabrication facility and thus can be suitable for lab-on-chip integration.

6 Conclusion

In this work, a small group of photonic biosensors have been studied, based on cascade grating waveguides. The structure designed is easy to fabricate by using the conventional CMOS facilities. Insertion of a cavity between the two segments of the grating waveguides provides a narrow resonant peak of high Q factor, of the order of 10^5. The sensor operates through observing the wavelength shift, and an almost linear dependence has been found between the resonant wavelength shift and the refractive index change of the biomaterial used. The impact of temperature on the detection of the chosen biomaterial (through its water content) has also been studied. The result shows a 0.12 nm resonant wavelength shift, over the temperature range of 34 ^{o}C to 18 ^{o}C. The results obtained show that making a compact size sensor that can be used for applications for lab-on-chip use for the simultaneous detection of several different biomaterials is possible.

Acknowledgement

The authors would like to acknowledge the mutual understanding for joint and collaborative work among researchers from Malaviya National Institute of Technology Jaipur (INDIA), Universiti Teknologi Malaysia, Johor Bahru, (MALAYSIA) and the Ton Duc Thang University, Ho Chi Minh City (VIETNAM). The support of the Royal Academy of \Engineering and the George Daniels Educational Trust is greatly appreciated.

References

Fan, X., White, I.M., Shopova, S.I., Zhu, H., Suter, J.D., Sun, Y.: Sensitive optical biosensors for unlabeled targets: A review. Anal. Chim. Acta. 620, 8–26 (2008). doi:10.1016/j.aca.2008.05.022

Zinoviev, K., Carrascosa, L.G., Del Río, J.S., Sepúlveda, B., Domínguez, C., Lechuga, L.M.: Silicon photonic biosensors for lab-on-a-chip applications. Adv. Opt. Technol. (2008). doi:10.1155/2008/383927

Estevez, M.C., Alvarez, M., Lechuga, L.M.: Integrated optical devices for lab-on-a-chip biosensing applications. Laser Photon. Rev. 6, 463–487 (2012). doi:10.1002/lpor.201100025

Chiu, M.-H., Wang, S.-F., Chang, R.-S.: D-type fiber biosensor based on surface-plasmon resonance technology and heterodyne interferometry. Opt. Lett. 30, 233–235 (2005). doi:10.1364/OL.30.000233

Ni, B., Chen, X.Y., Xiong, D.Y., Liu, H., Hua, G.H., Chang, J.H., Zhang, J.H., Zhou, H.: Infrared plasmonic refractive index-sensitive nanosensor based on electromagnetically induced transparency of waveguide resonator systems. Opt. Quantum Electron. 47, 1339–1346 (2015). doi:10.1007/s11082-014-0059-0

Azzam, S.I., Hameed, M.F.O., Shehata, R.E.A., Heikal, A.M., Obayya, S.S.A.: Multichannel photonic crystal fiber surface plasmon resonance based sensor. Opt. Quantum Electron. 48, 1–11 (2016). doi:10.1007/s11082-016-0414-4

Mohanty, G., Sahoo, B.K., Akhtar, J.: Comparative analysis for reflectivity of graphene based SPR biosensor. Opt. Quantum Electron. 47, 1911–1918 (2015). doi:10.1007/s11082-014-0057-2

Boyd, R.W., Heebner, J.E.: Sensitive disk resonator photonic biosensor. Appl. Opt. 40, 5742–5747 (2001). doi:10.1364/AO.40.005742

Guider, R., Gandolfi, D., Chalyan, T., Pasquardini, L., Samusenko, A., Pucker, G., Pederzolli, C., Pavesi, L.: Design and optimization of SiON ring resonator-based biosensors for aflatoxin M1 detection. Sensors (Switzerland). 15, 17300–17312 (2015). doi:10.3390/s150717300

Dutta, H.S., Pal, S.: Design of a highly sensitive photonic crystal waveguide platform for refractive index based biosensing. Opt. Quantum Electron. 45, 907–917 (2013). doi:10.1007/s11082-013-9697-x

Derbali, J., AbdelMalek, F., Obayya, S.S.A., Bouchriha, H., Letizia, R.: Design of a compact photonic crystal sensor. In: Optical and Quantum Electronics. pp. 463–472 (2011)

Liu, Q., Tu, X., Kim, K.W., Kee, J.S., Shin, Y., Han, K., Yoon, Y.J., Lo, G.Q., Park, M.K.: Highly sensitive Mach-Zehnder interferometer biosensor based on silicon nitride slot waveguide. Sensors Actuators, B Chem. 188, 681–688 (2013). doi:10.1016/j.snb.2013.07.053

Sahu, S., Kozadaev, K. V, Singh, G.: Michelson Interferometer Based Refractive Index Biosensor. In: 13th International Conference on Fiber Optics and Photonics. p. Th3A.60. OSA, Washington, D.C. (2016)

Chen, Z., Flueckiger, J., Wang, X., Zhang, F., Yun, H., Lu, Z., Caverley, M., Wang, Y., Jaeger, N.A.F., Chrostowski, L.: Spiral Bragg grating waveguides for TM mode silicon photonics. Opt. Express. 23, 25295 (2015). doi:10.1364/OE.23.025295

Sahu, S., Ali, J., Singh, G.: Refractive index biosensor using sidewall gratings in dual-slot waveguide. Opt. Commun. 402, 408–412 (2017). doi:10.1016/j.optcom.2017.06.051

Wang, X., Flueckiger, J., Schmidt, S., Grist, S., Fard, S.T., Kirk, J., Doerfler, M., Cheung, K.C., Ratner, D.M., Chrostowski, L.: A silicon photonic biosensor using phase-shifted Bragg gratings in slot waveguide. J. Biophotonics. 6, 821–828 (2013). doi:10.1002/jbio.201300012

Sahu, S., Singh, G.: Modeling of grating slot waveguide for high-Q based refractive index sensor. In: 2017 International Conference on Computer, Communications and Electronics (Comptelix). pp. 394–396. IEEE (2017)

Prabhathan, P., Murukeshan, V.M., Jing, Z., Ramana, P. V: Compact SOI nanowire refractive index sensor using phase shifted Bragg grating. Opt. Express. 17, 15330 (2009) doi:10.1364/OE.17.015330.

Chrostowski, L., Hochberg, M.: Silicon Photonics Design. Cambridge University Press, Cambridge (2015)

Prabhathan, P., Murukeshan, V.M.: Silicon waveguide multiplexed sensor array configuration for label-free biosensing applications. J. Indian Inst. Sci. 94, 273–282 (2014)

Najafgholinezhad, S., Olyaee, S.: A photonic crystal biosensor with temperature dependency investigation of micro-cavity resonator. Optik (Stuttg). 125, 6562–6565 (2014). doi:10.1016/j.ijleo.2014.08.043

Talebi Fard, S., Grist, S.M., Donzella, V., Schmidt, S.A., Flueckiger, J., Wang, X., Shi, W., Millspaugh, A., Webb, M., Ratner, D.M., Cheung, K.C., Chrostowski, L.: Label-free silicon photonic biosensors for use in clinical diagnostics. 8629, 862909 (2013). doi:10.1117/12.2005832

Gonzalo Wangüemert-Pérez, J., Cheben, P., Ortega-Moñux, A., Alonso-Ramos, C., Pérez-Galacho, D., Halir, R., Molina-Fernández, I., Xu, D.-X., Schmid, J.H.: Evanescent field waveguide sensing with subwavelength grating structures in silicon-on-insulator. Opt. Lett. 39, 4442 (2014). doi:10.1364/OL.39.004442

Wang, X., Grist, S., Flueckiger, J., Jaeger, N.A.F., Chrostowski, L.: Silicon photonic slot waveguide Bragg gratings and resonators. Opt. Express. 21, 19029 (2013). doi:10.1364/OE.21.019029

Bashkatov, A.N., Genina, E.A.: Water refractive index in dependence on temperature and wavelength: a simple approximation. Proc. SPIE 5068, Saratov Fall Meet. 2002 Opt. Technol. Biophys. Med. IV, 393 (October 14, 2003). 5068, 393–395 (2003). doi:10.1117/12.518857